NenuFAR Performance for Solar Radio Observations

C Briand, B Cecconi, N Chrysaphi, J N Girard, J.-M Grießmeier, K Hariharan, A Loh, P Murphy, K Sasikumar Raja, P Zarka, et al.

NenuFAR Performance for Solar Radio Observations

C. Briand, B. Cecconi, N. Chrysaphi, J. N. Girard, J.-M. Grießmeier, K. Hariharan, A. Loh, P. Murphy, K. Sasikumar Raja, P. Zarka, and P. Zhang

Abstract – NenuFAR is a new radio telescope covering the range 10 MHz to 85 MHz, implemented in France. It extends the capabilities of LOFAR toward the low-frequency range. The scientific goals are wide, from the dark ages of the universe and galaxies to pulsars and the search for exoplanets. This letter illustrates the capabilities of NenuFAR for solar studies.

1. Introduction

The sun is an active star. The activity manifests itself by transient eruptive phenomena, leading to, among others, the acceleration of energetic particles. Coherent radio emissions result from mildly relativistic electron beams either generated at reconnection sites during solar flares or accelerated during the propagation of interplanetary shocks [1]. Observed in the decameter range, these emissions provide the opportunity to diagnose the solar corona in a range of altitudes not reached by any spacecraft. Following the plasma emission hypothesis, electron beams are the source of free energy that destabilizes the plasma and generates electromagnetic waves at a frequency close to the local plasma frequency ω_p or its harmonic $2\omega_p$. The time-frequency drift that is often observed enables an estimate of the electron beam velocity (providing a density model). The degree of polarization of decameter radio emissions strongly varies, depending on the mechanism at play during the emission process. The degree of circular polarization is proportional to the ratio of the electron cyclotron frequency to the plasma frequency, providing an estimation of the weak coronal magnetic field, that is, in regions where other techniques fail [2]. In contrast to instruments working in the optical range, very high temporal resolution (a few tens of milliseconds) can be achieved with radio observations. Together with a very high spectral resolution, many fine structures are revealed within the time-frequency spectrum (the so-called dynamic spectrum). As recently shown, they can reveal the turbulent nature of the coronal density, and their duration and drift depend on the local temperature [3–6]. Combining radio measurements with other high-energy radiation observations (like γ-ray, X-ray, and extreme ultraviolet) efficiently provides clues to identify the sites of nonthermal electrons and to test the different models proposed to explain eruptive phenomena [7]. Finally, the decameter range is fundamental to linking the plasma of the corona to the plasma of the interplanetary medium observed mostly by space instruments.

This letter discusses the NenuFAR observing modes useful for solar studies. Section 2 describes some aspects of the instrument, while sections 3 and 4 show observations performed with the beam-forming mode and the imaging mode, respectively.

Manuscript received 29 September 2022.

C. Briand, B. Cecconi, N. Chrysaphi, J. N. Girard, A. Loh, P. Murphy, and P. Zarka are with LESIA/Observatoire de Paris-PSL, CNRS, Sorbonne Université, Université Paris-Cité, France.

N. Chrysaphi is with the School of Physics and Astronomy, University of Glasgow, United Kingdom (carine.briand@obspm.fr).

J. M. Grießmeier is with LPC2E, Université d'Orléans, CNRS, Orléans France, and ORN, Observatoire de Paris, Université PSL, Université d'Orléans, CNRS, Orléans, France.

K. Hariharan is with the University of Cape Town, Cape Town, South Africa, and Arizona State University, Tempe, Arizona, USA.

K. Sasikumar Raja is with the Indian Institute of Astrophysics, Bengaluru, India.

P. Zhang is with the Institute of Astronomy and National Astronomical Observatory, Bulgarian Academy of Sciences, Sofia, Bulgaria; ASTRON, Netherlands Institute for Radio Astronomy, Dwingeloo, the Netherlands; and the Astronomy and Astrophysics Section, Dublin Institute for Advanced Studies, Dublin, Ireland.

2. NenuFAR at a Glance

The New Extension in Nançay Upgrading LOFAR (NenuFAR) is a large low-frequency radio telescope recently deployed in France [8, 9]. It is a stand-alone phased array and interferometer as well as a low-frequency extension of LOFAR. It covers frequencies between 10 MHz and 85 MHz. The observations presented in this letter were obtained with 76 mini-arrays (MA) from the core (each MA is composed of 19 antennas) plus four distant MA for imaging (Figure 1). Thus, NenuFAR already has 1,444 core antennae in use in contrast to, for example, the 1,152 antennae of the complete LOFAR core. The collecting area is then 52,749 m^2 at 20 MHz and 5,996 m^2 at 85 MHz, the system equivalent flux density being 3,348 Jy at 20 MHz and 2,116 Jy at 85 MHz. Within an analog beam size, numerical summation enables pointing several beams simultaneously in different directions several degrees apart from the sun's center. Spectral and temporal resolution can be set down to $\delta f = 0.1$ kHz and/or $\delta t = 0.3$ ms. Each antenna is composed of two crossed dipoles, allowing polarization measurements in the four Stokes parameters. More instrumental details can be found in [10] and in the "Astronomer" section of the NenuFAR website (https://nenufar.obs-nancay.fr/en/homepage-en). Finally, the instrument longitudinal location enables continuity of solar observation for almost 24 h during dedicated campaigns with, for example, the Murchison WideField Array, observing

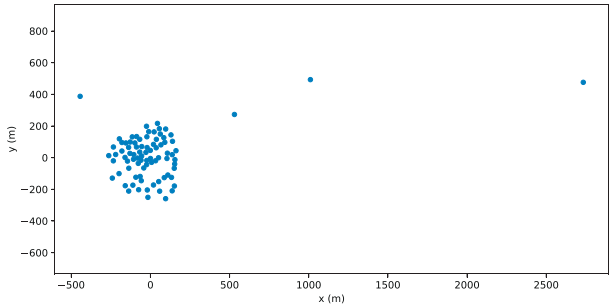

Figure 1. Distribution of each mini-array of the core and the four distant mini-arrays already in activity. The array's core is located at (x, y) = (6.6974E6, 6.6978E6) in the Lambert93 coordinate system.

between 70 MHz and 300 MHz from Australia, and the Long Wavelength Array, covering the range 10 MHz to 88 MHz and observing from the United States.

3. Beam-Forming Mode

3.1 Coronal Shocks

The shock-generated radio emissions, so-called Type II emissions, trace the plasma conditions encountered by the electron beams in the vicinity of the shock front. Despite many studies, the question of electron acceleration at shock is still debated. High spectral and temporal resolution spectra have revealed the presence of many fine structures [11–13] that enable characterization of the coronal plasma where shocks propagate. For example, the presence of herringbone emissions [14] can be explained by the formation of electron beams trapped between wavy-shock edges [5, 11, 15] or particle acceleration at termination shocks of reconnection sites [16, 17] or at shocks reflected at coronal hole boundaries [18].

During the Early Science phase of the instrument, two Type II radio bursts were observed, first on 28 March 2022 (Figure 2) and then on 19 May 2022

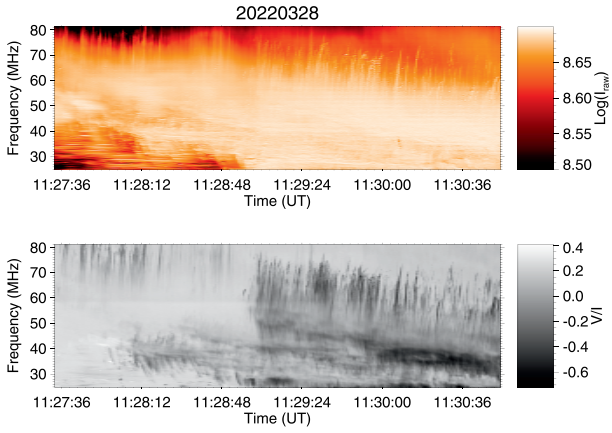

Figure 2. Part of the Type II emission observed on 28 March 2022. The top panel displays the Stokes I (arbitrary units), while the bottom panel displays Stokes V/I.

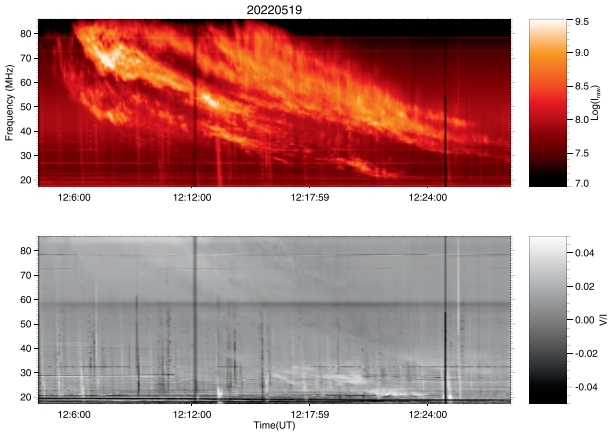

Figure 3. Type II emission from a shock occurring on 19 May 2022. Top panel: Stokes I (in arbitrary units); bottom panel: Stokes V/I. Many Type III, Type IIIb, and spikes are also observed and are better observed on the polarized spectrum since the polarization of the Type II is almost zero.

(Figure 3). The instrumental setup was equivalent in the two cases, with a temporal and spectral resolution of δt = 21 ms and δf = 3 kHz, respectively.

The Type II event of 28 March is related to an M4.0 flare starting at 1058 h and peaking at 1129 h, as recorded by GOES. A partial halo coronal mass ejection (CME) was also detected half an hour later (https://www.sidc.be/cactus/catalhttps://www.sidc.be/cactus/catalog/LASCO/2_5_0/qkl/2022/03/CME0090/CME.html). Several herringbone emissions are well observed in circular polarization (Stokes V/I; Figure 2, bottom panel). Note that the data are not yet corrected for leakage between Stokes parameters. As can be seen from the bottom panel of Figure 2, individual herringbones display intermittent emissions that can be related to the dynamics of electron beams and density fluctuations in the vicinity of the shock. The second Type II emission occurred on 19 May 2022, independent of any X-flare but producing a CME on the southwest limb (https://www.sidc.be/cactus/catalog/LASCO/2_5_0/qkl/2022/05/CME0119/CME.html). This Type II is highly structured: it is composed multiple lanes, with unclear fundamental-harmonic dependence. While some kind of herringbone structures are visible at high frequencies, no polarization is detected. The circular polarization of Type II is very low, which enables us to identify weak Types III, Type IIIb-III, and isolated-spike emissions.

3.2 Stria, Type IIIb, and Spikes

Short duration (less than 1 s), narrow-band (a few tens of kilohertz) emissions are often observed as isolated single or double strias (then called spikes or drift pair bursts) or forming chains before a Type III event (the so-called Type IIIb).

Stria properties strongly depend on the local temperature and the density of the emitting plasma [6, 19]. Figure 4 displays an exceptional sequence of

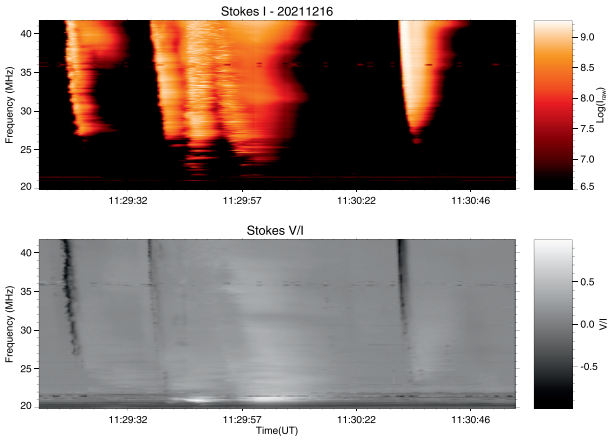

Figure 4. Stria chain and Type IIIb-III emission observed on 16 December 2021. Top panel: Stokes *I* (in arbitrary units); bottom panel: Stokes *V*/*I*.

extended stria chain and Type IIIb-III emissions. Their relatively long duration (several seconds) and almost null frequency drift suggest a temperature of about 1 MK [6]. Figure 5 displays another example of Type IIIb-III emission. The circular polarization signal (right panels) is fascinating first because it is very intense (suggesting that the emission is on the fundamental) and then because the polarity reverses with frequency (from negative to positive). Due to the high spectral and temporal resolution, local polarity reversals in scales of milliseconds and kilohertz are also observed (Figure 5, bottom right panel).

Emissions from isolated spikes often occur during eruptive periods. Type III duration is determined by both the collision rate (the duration of the photon excitation by the electron beam at the given location) and propagation effects. The small spatial extension of the electron beams related to spikes enables us to consider that the particle collision rate mostly domi-

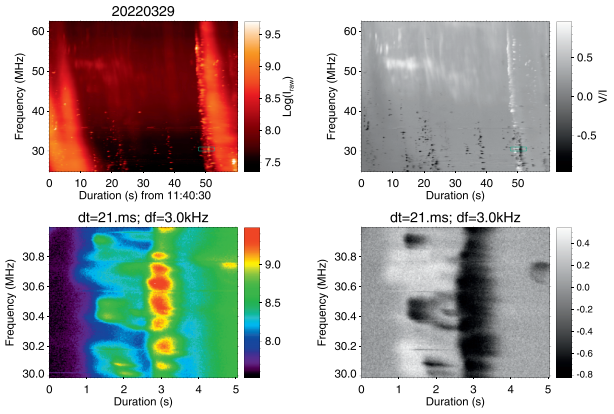

Figure 5. Details of emission within a Type IIIb-III chain. Left panels: Stokes *I* (arbitrary units); right panels: Stokes *V*/*I*. Top panels: dynamic spectra of 60 MHz s duration. The green frames indicate the location of the zoom presented on the bottom panels. The time resolution of the observation was 21 MHz ms, and the frequency resolution was 3 kHz.

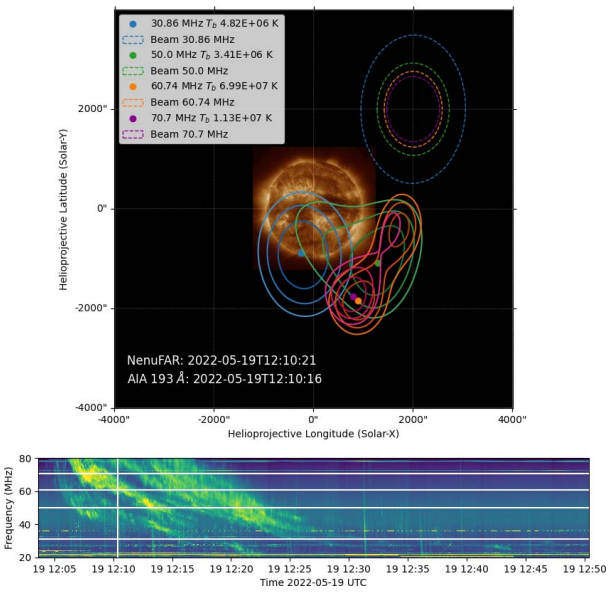

Figure 6. NenuFAR contours at 30.86 MHz, 50.0 MHz, 60.74 MHz, and 70.7 MHz from Type II presented in Figure 3 overlaid on an AIA 193 Å image. The beam size at each frequency is indicated on the top right of the image. The vertical white line on the bottom panel indicates the time of the image on the dynamical spectrum, while the horizontal lines denote the frequencies imaged.

nates their duration. This gives a clue to deducing the temperature of the particles during eruptive periods [19, 20].

4. Solar Imaging

Dynamic spectra are very useful for deducing several properties of the coronal plasma. However, while very high temporal and spectral resolutions are achieved, spatial resolution is moderate: the smallest beam size (25.2′) is of the order of the sun's diameter. Imaging appears like a powerful complementary observing mode, enabling us to follow the source-location time-evolution. For example, [11] recently studied the relationship between the expansion of CMEs, shocks, and particle acceleration by combining dynamic spectra and images at low frequencies with LOFAR. Also, [21] used high-cadence images together with dynamic spectra to disentangle the role of electron beam extension, density fluctuations, and scattering on the duration of Type III time profiles.

Apart from the MA of the NenuFAR's core, four distant MA are already operational, which greatly improves the instrument's imaging capacity. Figure 6 displays the first snapshots of a sequence of images from the Type II burst of 19 May 2022. The 1 MHz s time resolution of the images enables us to follow the dynamics of the radio source. After image processing, the angular resolution for this observation is $17.4' \times 21.6'$ at 70.7 MHz and $34.8' \times 49.2'$ at 30.86 MHz.

5. Conclusions

NenuFAR is very well adapted for solar observations. The instrumental resolution no longer limits the observations: fine structures of the emissions reveal the complexity of the coronal plasma. The exceptional high sensitivity reveals the presence of many emissions. Adding the polarimetric measurement capabilities, NenuFAR provides unprecedented observations of solar emissions at decametric frequencies. The imaging capabilities, together with the beam forming, provide new opportunities to locate the emission and to study the solar corona dynamics. NenuFAR's multibeam pointing allows for the simultaneous observation of the sun and the background sky. This, along with observations of known calibration sources (e.g., Cas-A and intercomparison with other calibrated instruments, such as the Nançay Decameter Array or LOFAR), will provide several ways to calibrate the instrument both in intensity and in polarimetry.

6. References

1. M. Pick, ‘‘Overview of Solar Radio Physics and Interplanetary Disturbances,” in D. E. Gary and C. U. Keller (eds.), *Solar and Space Weather Radiophysics*, Astrophysics and Space Science Library, Vol. 314, Berlin, Springer Science, 2004, pp. 17-45.
2. A. Willes and D. Melrose, “The Polarization of the Second Harmonic Coronal Type III Bursts,” *Solar Physics*, **171**, 2, 1997, pp. 393-418.
3. E. P. Kontar et al., “Anisotropic Radio-Wave Scattering and the Interpretation of Solar Radio Emission Observations,” *The Astrophysical Journal*, **884**, 2, 2019, doi: 10.3847/1538-4357/ab40bb.
4. X. Chen et al., “Subsecond Time Evolution of Type III Solar Radio Burst Sources at Fundamental and Harmonic Frequencies,” *The Astrophysical Journal*, **905**, 1, 2020, doi: 10.3847/1538-4357/abc24e.
5. E. P. Carley et al., “Observations of Shock Propagation Through Turbulent Plasma in the Solar Corona,” *The Astrophysical Journal*, **921**, 1, 2021, doi: 10.3847/1538-4357/ac1acd.
6. H. A. S. Reid and E. P. Kontar, “Fine Structure of Type III Solar Radio Bursts From Langmuir Wave Motion in Turbulent Plasma,” *Nature Astronomy*, **5**, 2021, pp. 786-804.
7. E. P. Carley, N. Vilmer, and A. Vourlidas, “Radio Observations of Coronal Mass Ejection Initiation and Development in the Low Solar Corona,” *Frontiers in Astronomy and Space Sciences*, **7**, 2020, pp. 79-99, doi: 10.3389/fspas.2020.551558.
8. P. Zarka et al., “The Low-Frequency Radio Telescope NeunFAR,” URSI GASS 2020, Rome, August 29–September 5, 2020.
9. P. Zarka et al., “LSS/NenuFAR: The LOFAR Super Station Project in Nançay,” Proceedings of the Annual Meeting of the French SF2A, Nice, December 2012, pp. 687-694.
10. L. Bondonneau et al., “Pulsars With NenuFAR: Backend and Pipelines,” *Astronomy and Astrophysics*, **652**, 2021, doi: 10.1051/0004-6361/202039339.
11. E. Morosan et al., “Multiple Regions of Shock-Accelerated Particles During a Solar Coronal Mass Ejection, *Nature Astronomy*, **3**, 2019, pp. 452-461, doi: 10.1038/s41550-019-0689-z.
12. N. Chrysaphi, H. A. S. Reid, and E. P. Kontar, “First Observation of a Type II Solar Radio Burst Transitioning Between a Stationary and Drifting State,” *The Astrophysical Journal*, **893**, 2, 2020, doi: 10.3847/1538-4357/ab80c1.
13. Magdalenić et al., “Fine Structure of a Solar Type II Radio Burst Observed by LOFAR,” *The Astrophysical Journal*, **897**, 1, 2020, doi: 10.3847/2041-8213/ab9abc.
14. I. H. Cairns and R. D. Robinson, “Herringbone Bursts Associated With Type II Solar Radio Emission,” *Solar Physics*, **111**, 2, 1987, pp. 365-383, doi: 10.1007/BF00148526.
15. E. P. Carley H. Reid, N. Vilmer, and P. T. Gallagher, “Low Frequency Radio Observations of Bi-Directional Electron Beams in the Solar Corona,” *Astronomy and Astrophysics*, **581**, 2015, doi: 10.1051/0004-6361/201526251.
16. H. Aurass, B. Vršnak, and G. Mann, “Shock-Excited Radio Burst From Reconnection Outflow Jet?,” *Astronomy and Astrophysics*, **384**, 2002, pp. 273–281, doi: 10.1051/0004-6361:20011735.
17. K-L. Klein et al., “The Relativistic Solar Particle Event on 28 October 2021: Evidence on Particle Acceleration in and Escape From Solar Corona,” *Astronomy and Astrophysics*, **663**, 2021, doi: 10.1051/0004-6361/202243903.
18. S. Mancuso, “Radio Evidence for a Shock Wave Reflected by a Coronal Hole,” *Astronomy and Astrophysics*, **651**, 2021, doi: 10.1051/0004-6361/202141387.
19. V. N. Melnik et al., “Solar Decameter Spikes,” *Solar Physics*, **289**, 5, 2014, pp. 1701-1714, doi: 10.1007/s11207-013-0434-1.
20. G. L. Tarnstrom and K. W. Philip, “Spike Burst—Type III Burst Associations,” *Astronomy and Astrophysics*, **17**, 1972, pp. 267-275.
21. P. Zhang, S. Yu, E. P. Kontar, and C. Wang, “On the Source Position and Duration of a Solar Type III Radio Burst Observed by LOFAR,” *The Astrophysical Journal*, **885**, 2, 2019, doi: 10.3847/1538-4357/ab458f.